3.2.3 de Haas-van Alphen effect

When we derived Landau orbital diamagnetic susceptibility, we took the small field limit, in that the Landau level splitting $\hbar\omega_c$ is much smaller than E_F and applied an asymptotic formula. When the magnetic field goes up to a comparatively large region [*1], the Landau quantization gives a dramatic effect on the magnetization. That is the oscillation of magnetization called the de Haas-van Alphen effect. In solids, the orbital diamagnetism strongly depends on the band structure particularly around the Fermi surface. This is in strong contrast to the spin paramagnetism. Hence the relation between the Pauli paramagnetism and the Landau diamagnetism shown in the previous subsection generally does not hold in solids. This sensitivity of diamagnetism to the band structure is applied for exploration of band structures.

We rewrite eq. (3.19) as

$$\frac{F}{n_e} = \mu - \frac{\hbar\omega_c}{E_F^{3/2}} \int_0^\infty dE \sum_{n=0} \left[E - \left(n + \frac{1}{2} \right) \hbar\omega_c \right]^{3/2} \left(-\frac{\partial f}{\partial E} \right), \tag{3.26}$$

where $n_e = N_e/L^3$. Also, the relation $2\mu_B B = \hbar\omega_c$ is used to restore $\hbar\omega_c$ in preparation for the change in the effective mass. The summation over n should be taken for positive arguments in the paretheses $(\cdots)$. On the other hand, the energy derivative of Fermi function $-\partial f \partial E$ approaches a delta function for $T \to 0$. We guess, therefore, the magnetization varies largely for the magnetic field where the Landau levels $(n+1/2)\hbar\omega_c$ coincide E_F. This oscillation of magnetization against the magnetic field is called **de Haas-van Alphen effect, dHvA effect**.

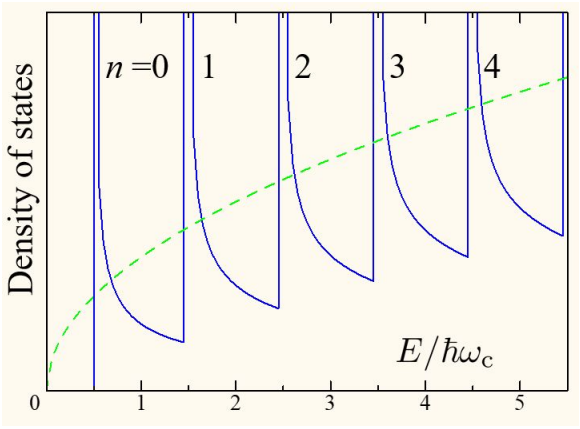

Fig. 3.2 Density of states is plotted against energy measured by Landau level spacing $\hbar\omega_c$.

The density of states of a one-dimensional system is given by

$$E_k = \frac{\hbar^2 k^2}{2m}, \quad \rho_{1d}(E) = \frac{1}{L}\frac{L}{2\pi}\left(\frac{\hbar^2 k}{m}\right)^{-1} = \frac{1}{2\pi\hbar}\sqrt{\frac{m}{2E}}.$$

By counting all these states, we get the total density of states per spin as

$$\rho(E) = \frac{1}{2\pi\hbar}\sqrt{\frac{m}{2}} \sum_{n=0} \frac{1}{\sqrt{(E-(n+1/2)\hbar\omega_c}}. \tag{3.27}$$

The summation over n should be taken for $E > (n+1/2)\hbar\omega_c$. The density of states in (3.27) is divergent at $E/\hbar\omega_c$ as shown in Fig. 3.2. With increasing magnetic field, the position of E_F decreases due to the increase in $\hbar\omega_c$. When E_F passes a position of divergence, a rapid rearrangement in electron population occurs and the thermodynamic functions including the magnetization get rapid changes.

To see how one can get the information of the Fermi surface, refer to Appendix 6B. In the lecture, I will introduce an example of experiment on Thallium-based high-Tc cuprate[1].

[*1] In usual metals, $\hbar\omega_c$ of "strong magnetic field" at an ordinary level does not go up to the level of Fermi energy. Hence even in this treatment, we still use the condition $\hbar\omega_c \ll E_F$

3.3 Orbital diamagnetism in graphene, graphite

What we have seen above is the magnetic response of the free electron system. The Pauli paramagnetism comes from a small shift of the spin bands on the energy axis. Hence we can guess that the same formula is applicable for band electrons in metals as long as the band has no anomaly at the Fermi level.

On the other hand, the orbital diamagnetism largely gets the effect of the band structure. Even in the low field limit, which is the constraint for the Landau diamagnetism, the magnetic response of Bloch electrons is a difficult problem. The theoretical frameworks from the viewpoint of linear response (Kubo formula)[2] and so forth have long been tried. The field is still active and there have been reports on theoretical developments aiming at application to graphene from this department[3, 4, 5]. Here I would like to introduce shortly a characteristic example of graphene and multilayer graphene (thin graphite). In the beginning of the present chapter, I have introduced the fact that a graphite has a very large negative orbital susceptibility. This is due to its characteristic band structure.

3.3.1 Orbital diamagnetism in graphene

We are familiar with **graphite**, e.g., as a material used in cores of pencils. It is said to be the most stable thermodynamically as elementally crystal of carbon. It's crystal structure is a stack of honeycomb planes as shown in Fig. 3.3. A single atomic layer of the graphite is called **graphene**, which can be extracted by exfoliation, grown by CVD, or thermalization of SiC.

Carbon atoms in a plane of graphene are strongly connected to the neighbors by covalent bonds with no buckling. Hence graphene conduction electrons in p_z orbitals can be treated as a complete two-dimensional orbital system. And just at $E_{\rm F}$ in pure graphenes, the linear dispersions form crossing points called **Dirac points** as shown in Appendix 6C. Hence the band is massless and gapless. The orbital susceptibility of graphene has long been calculated. In the simplest model[6], it is given by (in cgs unit)

$$\chi(E_{\rm F}) = -\frac{g_v g_s e^2}{6\pi}\left(\frac{e}{c}\right)^2 \delta(E_{\rm F}), \tag{3.28}$$

where $g_v = 2$ is the orbital degeneracy represented as K and K' points in k-space, $g_s = 2$ is the spin degeneracy, c is the speed of light. Here $E_{\rm F}$ is measured from the Dirac points, and the susceptibility in (3.28) is infinite when $E_{\rm F}$ is at the Dirac points, and is zero elsewhere.

This can be roughly interpreted as follows. Let an electron be in a cyclotron motion (thus not at Dirac points) under a magnetic field B. When B changes, an electric field E is created as in eq. (1.28). In sec. 1.3.2, E accelerates the electron resulting in the diamagnetism. In the present case, E gives an increase in the kinetic energy of the electron though that does not enhance the velocity due to the linear dispersion. Hence the diamagnetic susceptibility is zero. However, when

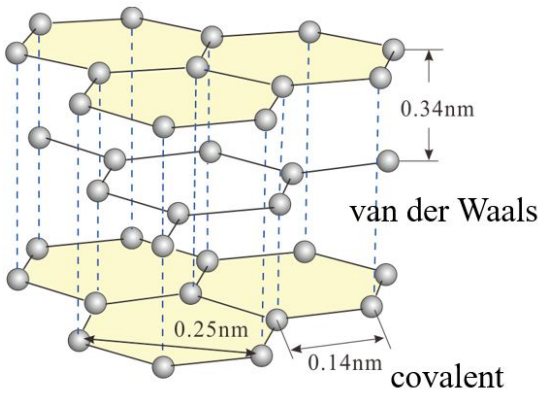

Fig. 3.3 Illustration of graphite crystal structure. Honeycomb sheets made of carbon covalent bonds are stacked with an in-plane half lattice constant shift by layer. That is, the same 2-dimensional lattice appears alternatively, which structure is called AB-stacking. The sheet-to-sheet is connected by the van der Waals coupling.

the increase in the energy goes over a Dirac point, the velocity jumps, e.g., from $-v_{\rm e}$ to $+v_{\rm e}$. The acceleration is infinite giving the divergence of the susceptibility at the Dirac point.

In the lecture I would like to introduce an experiment, in which the authors claim they have observed such peculiar orbital diamagnetic susceptibility of graphene.

3.3.2 Diamagnetic susceptibility of multi-layer graphene

The extraordinary diamagnetism that causes magnetic levitation, and the strong magneto-optical response have long been known, but clear interpretations have not been given yet. It has been said that we need to consider a more practical model, in which experimental details like inhomogeneity in the field[7].

In order to treat the space distribution of magnetic field, we consider the Fourier expansion in x: $B(\boldsymbol{r}) = B(q)\cos qx$, of the field along z-axis onto 2-dimensional system in xy-plane. The current distribution in response to $B(\boldsymbol{r})$ generally has the form of $j_y(\boldsymbol{r}) = j_y(q)\sin qx$[9]. The q-component of magnetization $m(\boldsymbol{r})$ is obtained from the two-dimensional current as この 2 次元電流から，磁化 $m(\boldsymbol{r})$ の q 成分は

$$j_y = -c\frac{\partial m}{\partial x} \to m(\boldsymbol{r}) = m(q)\cos qx \quad m(q) = -\frac{j_y(q)}{cq}.$$

The susceptibility $\chi(q)$ is defined as $m(q)/B(q)$. Then the response current of graphene to $B(\boldsymbol{r}) = B(q)\cos qx$ is

$$j_y(\boldsymbol{r}) = -\frac{g_v g_s e^2 v}{16\hbar c}B(q)\sin qx. \tag{3.29}$$

The diamagnetic inductive current by this responding current is from Amperé's law

$$B_{\rm ind}(\boldsymbol{r}) = -\alpha_g B(\boldsymbol{r}), \quad \alpha_g = \frac{2\pi g_v g_s e^2 v}{16\hbar c^2} \approx 4\times 10^{-5}, \tag{3.30}$$

which does not depend on the space distribution wavenumber q. Therefore any spatial distribution of magnetic field causes the inductive magnetic field of $-\alpha_g$ times the original field and the theorem of superposition leads to the total inductive field of $-\alpha_g$ times the total original field.

As an example, let us place a magnetic charge $q_{\rm m}$ in the region $z > 0$. The graphene at $z = 0$ partially screens the field to create the mirror charge $-\alpha_q q_{\rm m}$ seen from $z < 0$, namely the field caused by the mirror charge is superposed to the original field. The same for $z > 0$ and the field created by the mirror charge of $\alpha_q q_{\rm m}$ in $z < 0$ region is overlapped to the original field. The force, which the original magnetic charge in Fig. 3.4(a) gets from the graphene, is calculated from the mirror charge in Fig. 3.4(c).

Let us consider the case a permanent magnet approaches a graphene. The magnet is a half-infinite cylinder with a radius a having the edge magnetic charge density σ_m. When the edge reaches the graphene, $d = 0$, the force given to the magnet per area is $2\pi\alpha_g\sigma_m^2$. In the case of Neodymium magnet, σ_m can be around 1 T. The force is then 0.16 dyne, which is surprisingly large for a single atomic layer.

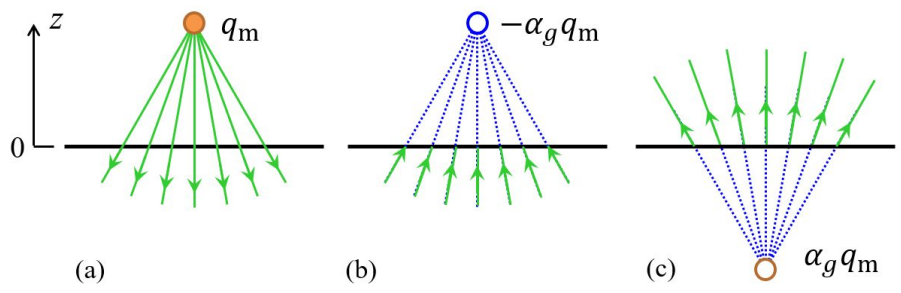

Fig. 3.4 Mirror magnetic charge caused by a graphene. The graphene is illustrated as the black line at $z = 0$. (a) Magnetic field by a magnetic charge. (b) Inducted field in $z < 0$, (c) and in $z > 0$. From [8].

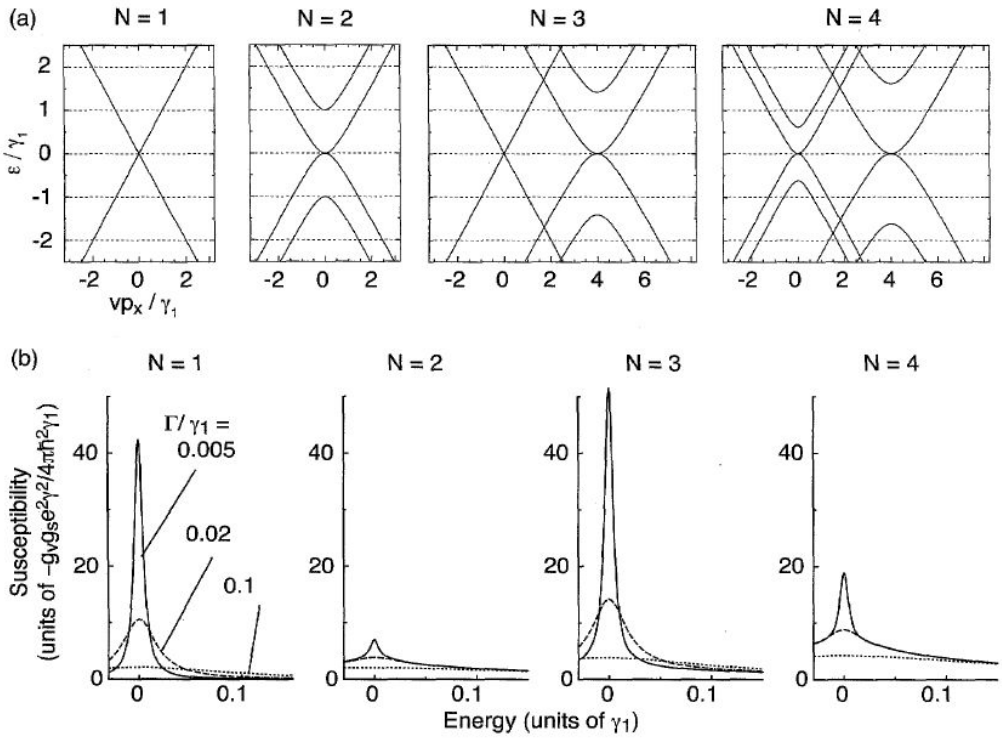

Fig. 3.5 (a) Band structures and (b) orbital diamagnetic susceptibilities $\chi(E_{\rm F})$ for single to four layer graphenes. Γ is the width of energy fluctuation caused by impurities. From [8, 10].

In an ordinary 2-dimensional metal with an effective mass m^*, the susceptibility is a constant $\chi_0 = -e^2/(24\pi m^* c^2)$ in the long wavelength limit. Let us take an example of GaAs 2-dimensional electrons with $m^* = 0.067 m_0$. Then the ratio of repulsive force f_c to that of graphene f_g is $f_g/f_c \approx a/(0.01\ \mathrm{nm})$. The radius is in cm order then the ratio goes up to 9-digits.

Next we go to multi-layer graphenes, which can be seen as thin films of graphite[10]. They have the AB stacking as in Fig. 3.3 with a weak interlayer coupling with the coupling energy of 0.4 eV. The structure with more layers than two, can be treated as a repetition of the AB stack and the calculation can be reduced to the case of the bilayer graphene. A single-layer graphene has gapless linear dispersion both at K and K'. Also in a bilayer graphene, a pair of bands has a zero-gap with finite effective masses, the other pair has a gap due to the inter-layer coupling. An $N = 2M$ layer graphene has M sets of bilayer-type bands. When $N = 2M + 1$, a set of single-layer bands is added.

Figure 3.5 shows such calculation of the band structures and the orbital diamagnetic susceptibilities for single to four layer graphenes. The band with a Dirac point appears for an odd number of N giving a large contribution to the diamagnetic susceptibility. For an even N, that contribution disappears. However the further increase in the number of layers results in the increase in the diamagnetic susceptibility. This increase is thought to lead to the large diamagnetism in graphite.

Chapter 4

Interaction between Spins

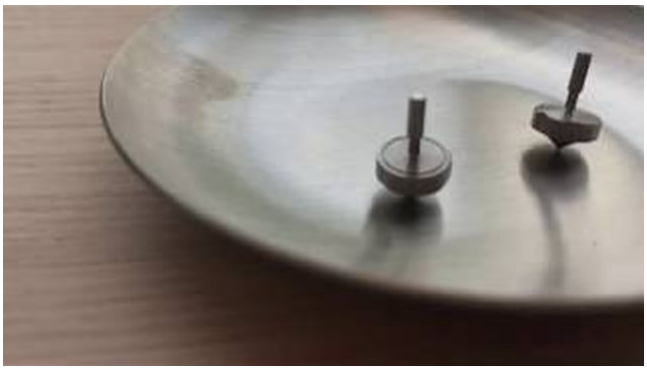

Fighting tops

https://www.youtube.com/watch?v=2WaU7NDOHLQ

We have looked for "entities" which work as magnetic dipoles in materials and found in the quantum theory, that the spins and the orbitals are working as magnetic dipoles namely magnetic moments in various forms. However the macroscopic moments never appear without applying external magnetic field due to the randomness in the direction of microscopic moments. In ferromagnetic materials the microscopic moments – let us call them spins – are aligned in the same direction at zero magnetic field and at finite temperatures. This fact indicates that, as we have seen in the magnetic refrigeration, the entropy is largely reduced and there should be a large decrease in the internal energy to compensate that. In other words, there should be some interaction that decreases the total energy. Let us examine such possibilities.

4.1 Exchange interaction

In chapter 1, we introduced the classical interaction between two magnetic dipoles (spins) $\boldsymbol{\mu}_1$, $\boldsymbol{\mu}_2$, namely the moments feel their magnetic field each other. Let $\boldsymbol{r}_{12}$ be the vector connecting the two moments, then the potential is given by [*2]

$$U(\boldsymbol{\mu}_1, \boldsymbol{\mu}_2, \boldsymbol{r}_{12}) = \frac{\mu_0}{4\pi}\left[\frac{\boldsymbol{\mu}_1 \cdot \boldsymbol{\mu}_2}{r_{12}^3} - 3\frac{(\boldsymbol{r}_1 \cdot \boldsymbol{r}_{12})(\boldsymbol{r}_2 \cdot \boldsymbol{r}_{12})}{r_{12}^5}\right]. \tag{4.1}$$

It is easy to guess from the analogy of bar magnets that the stable configuration is that the two spins are in-line. However this has the quantitative problem. Let $\boldsymbol{\mu}_{1,2}$ be $5\mu_\mathrm{B}$, r_{12} be 200 pm (typical lattice constant), then U is about 2 K. Hence this interaction cannot explain real ferromagnets, which keep alignments of spins above room temperature quantitatively.

Based on the quantum theory, Heisenberg showed the possibility of far-stronger mutual interaction between spins, that comes from a characteristic quantum effect[11]. It is now known through various researches that the direct exchange interaction, which Heisenberg claimed to be the source of ferromagnetism, cannot explain real ferromagnetism in materials. However, the concept of exchange interaction is still used in the present understandings. Here let us introduce the naive direct exchange interaction.

[*2] In eq. (1.7), we used E-H formulation. Here we restore it to E-B formulation (i.e., SI unit system).

4.1.1 Heitler-London approximation

In the ground state of Hydrogen molecule, two electrons with $\uparrow$ and $\downarrow$ are accommodated in the bonding orbital. Hence the spin is zero and the orbital diamagnetism appears (molecular orbital approximation, MO). However, here we consider the case that the inter-atom distance is larger and instead of considering bonding and anti-bonding orbitals, we consider atomic orbitals φ_a, φ_b and the two-body wavefunction is composed with keeping the Fermi statistics (**Heitler-London approximation**). In this approximation, the wavefunction of two electrons is written in the form of Slater determinant:

$$\Psi = \frac{1}{\sqrt{N}} \begin{vmatrix} \varphi_a(\boldsymbol{r}_1)\chi_a(s_1) & \varphi_b(\boldsymbol{r}_1)\chi_b(s_1) \\ \varphi_a(\boldsymbol{r}_2)\chi_a(s_2) & \varphi_b(\boldsymbol{r}_2)\chi_b(s_2) \end{vmatrix}, \tag{4.2}$$

where N is a normalization constant, $(\boldsymbol{r}_i, s_i)$ are space and spin coordinates of i-th electron. s_i corresponds to z-component of spin and can take one of two values $\pm 1/2$. We write the state of the spin pointing $+z$ as $\alpha(s)$, in which $\chi(s)$ is

$$\chi(1/2) = 1, \quad \chi(-1/2) = 0. \tag{4.3}$$

On the other hand, the $-z$ pointing state $\beta(s)$ is given as

$$\chi(1/2) = 0, \quad \chi(-1/2) = 1. \tag{4.4}$$

Pauli's exclusion principle is fulfilled as

$$\Psi(\boldsymbol{r}_1, s_1; \boldsymbol{r}_1, s_1) = 0, \quad \Psi(\boldsymbol{r}_1, s_1; \boldsymbol{r}_2, s_2) = -\Psi(\boldsymbol{r}_2, s_2; \boldsymbol{r}_1, s_1). \tag{4.5}$$

Ψ takes argument of spin functions (χ_a, χ_b), and we can classify Ψ by the spin states (α, β) as $\{\Psi_{\alpha\alpha}, \Psi_{\alpha\beta}, \Psi_{\beta\alpha}, \Psi_{\beta\beta}\}$. We take this as a basis and consider the expression of the interaction Hamiltonian $\mathscr{H}_{\rm int}$. As an example of the matrix elements, $\langle\alpha\alpha|\mathscr{H}_{\rm int}|\alpha\alpha\rangle$ has two terms:

$$\begin{aligned} \langle\alpha\alpha|\mathscr{H}_{\rm int}|\alpha\alpha\rangle &= \sum_{s_1,s_2} \int d\boldsymbol{r}_1 d\boldsymbol{r}_2 \Psi^*_{\alpha\alpha} \mathscr{H}_{\rm int} \Psi_{\alpha\alpha} \\ &= \int d\boldsymbol{r}_1 d\boldsymbol{r}_2 \varphi^*_a(\boldsymbol{r}_1)\varphi^*_b(\boldsymbol{r}_2)\mathscr{H}_{\rm int}\varphi_a(\boldsymbol{r}_1)\varphi_b(\boldsymbol{r}_2) - \int d\boldsymbol{r}_1 d\boldsymbol{r}_2 \varphi^*_a(\boldsymbol{r}_1)\varphi^*_b(\boldsymbol{r}_2)\mathscr{H}_{\rm int}\varphi_b(\boldsymbol{r}_1)\varphi_a(\boldsymbol{r}_2), \end{aligned} \tag{4.6}$$

where we take $N = 2$, $\langle\varphi_a|\varphi_b\rangle = 0$. The second term in rhs of (4.6) is a matrix element between the states in which the electrons are exchanged, and called **exchange integral**. This is essentially the same as $J(m_1, m_2)$ in eq. (2.26). In Ch.2, we derived Hund's rule from this integral. The direct exchange interaction is essentially the same. We write the first and the second term in rhs of eq. (4.6) as K_{ab} and J_{ab}. The 4×4 matrix elements are as follows.

	$\alpha\alpha$	$\alpha\beta$	$\beta\alpha$	$\beta\beta$
$\alpha\alpha$	$K_{ab} - J_{ab}$	0	0	0
$\alpha\beta$	0	K_{ab}	$-J_{ab}$	0
$\beta\alpha$	0	$-J_{ab}$	K_{ab}	0
$\beta\beta$	0	0	0	$K_{ab} - J_{ab}$

(4.7)

This can be easily diagonalized and the eigenfunctions are

$$\left.\begin{matrix} \Psi_{\alpha\alpha} \\ \frac{1}{\sqrt{2}}(\Psi_{\alpha\beta} + \Psi_{\beta\alpha}) \\ \Psi_{\beta\beta} \end{matrix}\right\} (s_1 + s_2 = 1), \quad \frac{1}{\sqrt{2}}(\Psi_{\alpha\beta} - \Psi_{\beta\alpha})\ (s_1 + s_2 = 0). \tag{4.8}$$

The three states for $s_1 + s_2 = 1$ are **spin triplet** and the one for $s_1 + s_2 = 0$ is **spin singlet**. The eigenenergy of the former is $K_{ab} - J_{ab}$ and that of the latter is $K_{ab} - J_{ab}$. The spin states thus give the difference in the energy. When

J_{ab} is positive, the spin parallel state has a lower energy giving ferromagnetic interaction while the interaction is anti-ferromagnetic when J_{ab} is negative. The situation can be viewed as the exchange integral creates the interaction between the spins and we call the interaction **exchange interaction**. Though J_{ab} appears from the integration of orbital states, the symmetry of the electronic states requires the interaction between spins.

Then we look for an effective Hamiltonian composed of spin operators just like the spin Hamiltonian introduced in Ch.2 to analyze EPR experiments. First we introduce spin operators $\boldsymbol{s}_a$ and $\boldsymbol{s}_b$, which operate on the states a and b respectively (don't get confused with s_1, s_2). Because they commute each other,

$$2\boldsymbol{s}_a \cdot \boldsymbol{s}_b = (\boldsymbol{s}_a + \boldsymbol{s}_b)^2 - \boldsymbol{s}_a^2 - \boldsymbol{s}_b^2 = \boldsymbol{S}^2 - \boldsymbol{s}_a^2 - \boldsymbol{s}_b^2. \tag{4.9}$$

Here we use

$$\langle\uparrow\uparrow|\boldsymbol{S}^2|\uparrow\uparrow\rangle = S(S+1) = 2, \quad \boldsymbol{S}^2|\uparrow\downarrow\rangle = 0, \tag{4.10}$$

$$\boldsymbol{s}_a^2 = \boldsymbol{s}_b^2 = \frac{1}{2}\left(\frac{1}{2}+1\right) = \frac{3}{4}, \tag{4.11}$$

and calculate the elements of operator $(1 + 4\boldsymbol{s}_a \cdot \boldsymbol{s}_b)/2$ to obtain

$$(\uparrow\uparrow) \to 2\boldsymbol{s}_a \cdot \boldsymbol{s}_b = 2 - 2 \times \frac{3}{4} = \frac{1}{2} \Longrightarrow \frac{1}{2}(1 + 4\boldsymbol{s}_a \cdot \boldsymbol{s}_b) = +1,$$
$$(\uparrow\downarrow) \to 2\boldsymbol{s}_a \cdot \boldsymbol{s}_b = 2 - 2 \times \frac{3}{4} = -\frac{3}{2} \Longrightarrow \frac{1}{2}(1 + 4\boldsymbol{s}_a \cdot \boldsymbol{s}_b) = -1.$$

Therefore we can adopt

$$\mathscr{H}_{\text{int}} = K_{ab} - \frac{1}{2}J_{ab}(1 + 4\boldsymbol{s}_a \cdot \boldsymbol{s}_b) \tag{4.12}$$

as an effective Hamiltonian.

Then we expand the above concept to the interaction between general spins $\boldsymbol{S}_i$ indexed by i and formally extract the spin part to obtain **Heisenberg Hamiltonian**

Heisenberg Hamiltonian

$$\mathscr{H} = -2\sum_{\langle i,j\rangle} J_{ij}\boldsymbol{S}_i \cdot \boldsymbol{S}_j. \tag{4.13}$$

This is an important basics for us to treat various phenomena originated from the interaction between spins.

For exchange integral, when the interaction is the Coulomb repulsion,

$$J_{ab} = \frac{e^2}{4\pi\epsilon_0}\int d\boldsymbol{r}_1 d\boldsymbol{r}_2 \varphi_a^*(\boldsymbol{r}_1)\varphi_b^*(\boldsymbol{r}_2)\frac{1}{r_{12}}\varphi_b(\boldsymbol{r}_1)\varphi_a(\boldsymbol{r}_2) \tag{4.14}$$

is always positive, which can be proven as eq. (2.26). And J_{ab} can go up to 0.1 eV depending on the way of estimation, hence might explain the room temperature ferromagnetism. In the above we see that the Coulomb repulsion causes a strong ferromagnetic interaction between spins in Heitler-London approximation. This is called **direct exchange interaction**. However, here we must notice that if we adopt the molecular orbital method, the interaction in the form of Heisenberg Hamiltonian can be derived with negative J, that is the anti-ferromagnetic interaction. This can be more easily understood from the general theory that in a general Schrödinger equation, the ground state has no degeneracy and the wavefunction has no node[12]. Hence the orbital part of wavefunction is symmetric resulting in the antisymmetric spin part.

4.1.2 Exchange interaction in the presence of tunneling

As an improvement of Heitler-London approximation, we consider the electronic state, in which two electrons are accommodated in a single atom as a possible configuration. In this treatment, a small amplitude of wavefunction

$$\Psi' = \frac{1}{\sqrt{N'}} \begin{vmatrix} \varphi_a(\boldsymbol{r}_1)\chi_a(s_1) & \varphi_a(\boldsymbol{r}_1)\chi'_a(s_1) \\ \varphi_a(\boldsymbol{r}_2)\chi_a(s_2) & \varphi_a(\boldsymbol{r}_2)\chi'_a(s_2) \end{vmatrix} \tag{4.15}$$

is overlapped to the one in (4.2). The transition of $\Psi \to \Psi'$ means tunneling of an electron $\varphi_b\chi_b \to \varphi_a\chi'_a$. Hence for such a superposition to occur, $\langle\Psi|\mathscr{H}|\Psi'\rangle \neq 0$. For that, due to Pauli's exclusion principle, χ_a and χ_b should be the spins opposite to each other. When $\boldsymbol{s}_a$ and $\boldsymbol{s}_b$ are anti-parallel, this hopping process leads to the energy decrease

$$W_{ab} = -\frac{1}{\Delta E} |\langle\Psi'|\mathscr{H}|\Psi\rangle|^2 \tag{4.16}$$

in the second order perturbation. For parallel spins, there is no such energy decrease. We thus write this part formally

$$\frac{1}{2}(1 - 4\boldsymbol{s}_a \cdot \boldsymbol{s}_b)W_{ab}, \tag{4.17}$$

which is in the same form as eq. (4.12). In summary we reach

$$\mathscr{H}'_{\rm int} = \frac{1}{2}(-J_{ab} + W_{ab}) - 2(J_{ab} + W_{ab})\boldsymbol{s}_a \cdot \boldsymbol{s}_b. \tag{4.18}$$

W_{ab} is negative and when $J_{ab} + W_{ab} < 0$ the total interaction becomes antiferromagnetic. We have confirmed Heitler-London approximation overestimates the ferromagnetic interaction.

Appendix 6A: Aharonov-Bohm phase and degeneracy of Landau levels

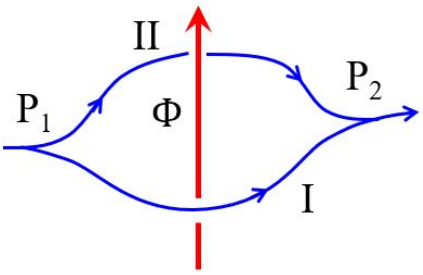

I would like to introduce the way to memorize the degree of Landau level degeneracy (the number of states per unit area). Of course this is just an example, and you can find your own way. In the existence of magnetic field, the momentum $\hbar\boldsymbol{k}$ is modified to

$$\hbar\boldsymbol{k} \ \to \ \hbar\boldsymbol{k} + e\boldsymbol{A} = \hbar\left(\boldsymbol{k} + \frac{e}{\hbar}\boldsymbol{A}\right).$$

This gives the phase evolution θ when a plane wave $\exp[i\boldsymbol{k}\cdot\boldsymbol{r}]$ propagates in space from a point P_1 to P_2 as

$$\theta_{12} = \int_{\mathrm{P}_1}^{\mathrm{P}_2} \left(\boldsymbol{k} + \frac{e}{\hbar}\boldsymbol{A}\right) \cdot d\boldsymbol{r}_{(\mathrm{I})} = \int_{\mathrm{P}_1}^{\mathrm{P}_2} \boldsymbol{k} \cdot d\boldsymbol{r}_{(\mathrm{I})} + \frac{e}{\hbar}\int_{\mathrm{P}_1}^{\mathrm{P}_2} \boldsymbol{A} \cdot d\boldsymbol{r}_{(\mathrm{I})} = \theta^{(k)}_{12(\mathrm{I})} + \theta^{(A)}_{12(\mathrm{I})}. \tag{6A.1}$$

The suffix I means the path signed as I in the figure. The first term in the rhs is the ordinary kinetic phase and the second term expresses the effect of magnetic field. The latter is called **Aharonov-Bohm** (AB) phase.

In path II, the kinetic phase differs from that in path I by the difference in the length. The AB phase in path II is also different from that in I. This can be understood by considering the route going back from P_2 to P_1 on path II. That is

$$\Delta\theta_{\rm AB} = \frac{e}{\hbar}\left[\int_{\mathrm{P}_1}^{\mathrm{P}_2} \boldsymbol{A} \cdot d\boldsymbol{r}_{(\mathrm{I})} + \int_{\mathrm{P}_1}^{\mathrm{P}_2} \boldsymbol{A} \cdot d\boldsymbol{r}_{(\mathrm{II})}\right] = \frac{e}{\hbar}\oint \boldsymbol{A} \cdot d\boldsymbol{r} = \frac{e}{\hbar}\int_S \mathrm{rot}\boldsymbol{A} d\boldsymbol{\sigma} = 2\pi\frac{\Phi}{\phi_0}, \quad \phi_0 = \frac{h}{e}. \tag{6A.2}$$

Here ϕ_0 is called **flux quantum**, which has the form of the ratio of h to e. This is an easy-to-memorize form. A physical meaning is that 2π of AB phase is given to an electron going around this amount of flux, and this is the condition of quantization in the electron loop.

The number of states in the magnetic field of magnetic flux density B in two-dimensional system is given by the flux per unit area (i.e. B) divided by the flux quantum. That is,

$$N(B) = \frac{B}{h/e} = \frac{eB}{h} = \frac{eBm}{hm} = \frac{m}{h^2}(h\omega_{\rm c}) = \frac{m}{2\pi\hbar^2}(\hbar\omega_{\rm c}). \tag{6A.3}$$

Hence we can see the number of states per Landau level eB/h and the two-dimensional density of states $m/2\pi\hbar^2$ in a very clear way.

Appendix 6B: Contribution of k-slab to the dHvA effect

There are various equivalent way to explain the principle of the dHvA effect. In the explanation from the density of states as in the text, it is rather difficult to see the effect contains the information of k-space. Hence here we explain the effect in the way given in Ref. [13]. Here we consider free electrons with an isotropic effective mass for simplicity. Electrons are free in z-direction (field direction) and Landau-quantized in xy plane as in eq. (3.14). Hence we define quasi-Fermi energy as the kinetic energy in xy-plane for a fixed k_z, that is

$$E'_{\rm F} \equiv E_{\rm F} - \frac{\hbar^2 k_z^2}{2m}. \tag{6B.1}$$

And we treat the system as a set of two-dimensional electrons with the Fermi energy of $E'_{\rm F}$ under Landau quantization. In k-space, each k_z is assigned to such a virtual two-dimensional system.

Then we consider a slab with thickness δk_z in k-space corresponding to a k_z. We call the region k-slab. The density of states in a k-slab "per magnetic flux density" ξ is given by

$$\xi = \frac{1}{L}\frac{L}{2\pi}\delta k_z \frac{eB}{h}\frac{1}{B} = \frac{e}{4\pi^2\hbar}\delta k_z \quad \left(= \frac{\delta k_z}{2\pi}\frac{1}{\phi_0}\right), \tag{6B.2}$$

where we also use things mentioned in App. 6A. I have put a comment on this quantity as a formula in the last parentheses. $\phi_0 \equiv h/e$ is **flux quantum** introduced in App. 6A. At absolute zero, the Landau levels corresponding to the integer q which satisfies $(q+1/2)\hbar\omega_{\rm c} \le E'_{\rm F}$ are occupied. Let us write the maximum integer in q as $q_{\rm max}$ and the number of occupied Landau levels is $q_{\rm max}+1$. Then the number of electrons belong to this k-slab is

$$n_{\rm e}(k_{\rm z}) = (q_{\rm max}+1)\xi B \tag{6B.3}$$

per unit area in the real space.

With increasing B, $n_{\rm e}$ increases linearly in accordance with (6B.3), and when B exceeds the value determined by the condition

$$q_{\rm max} + \frac{1}{2} = \frac{E'_{\rm F}}{\hbar\omega_{\rm c}} = \frac{mE'_{\rm F}}{\hbar e}\frac{1}{B}, \tag{6B.4}$$

$q_{\rm max}$ decreases by one and $n_{\rm e}$ discretely decreases. Namely, $n_{\rm e}(k_{\rm z})$ oscillates periodically against $1/B$ and the amplitude (the amount of dropping at the condition (6B.4)) increases with B as ξB though the center of the oscillation is the electron concentration of virtual 2-dimensional electrons (let us write it $n_{\rm e0}$) in the k-slab before the application of magnetic field. The behavior is drawn in Fig. 6B.1. As shown in the figure, the electronic states of number eB/h at zero field are assigned to a Landau level (App. 6A). In the oscillation, at the magnetic field $n_{\rm e}(B) = n_{\rm e0}$, where the electron concentration hits the center, $(q_{\rm max}+1)(eB/h)$ should be equal to $n_{\rm e0}$. We write $q_{\rm max}+1$ at such points as ν, the value of magnetic field as B_ν. Then they are in the relation

$$B_\nu = \frac{1}{\xi}\frac{n_{\rm e0}}{\nu} = \frac{2\pi}{\delta k_z}\phi_0\frac{n_{\rm e0}}{\nu} \quad (\nu = 1, 2, \cdots). \tag{6B.5}$$

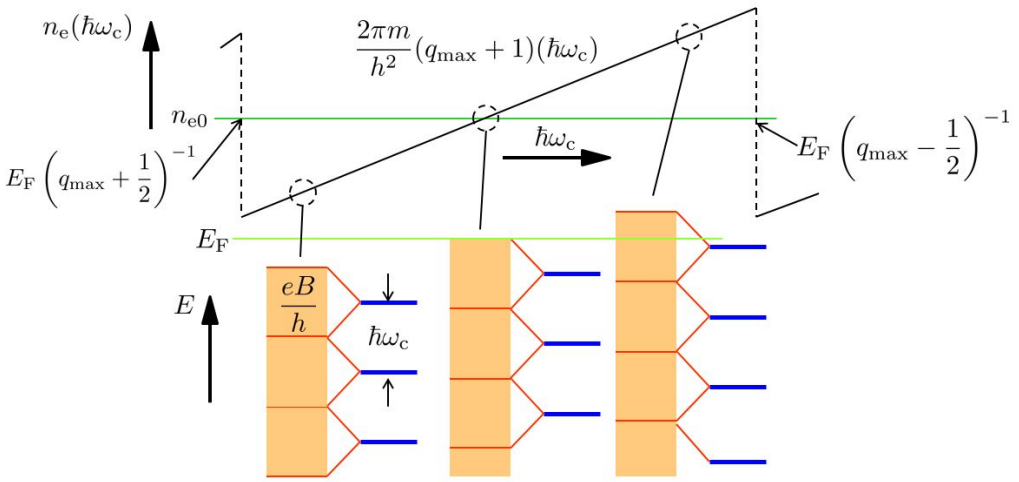

Fig. 6B.1 Illustration of relations between the Landau level distance $\hbar\omega_c$, the two dimensional electron concentration n_e, and jumping at which q_{max} changes. The lower shows corresponding energy diagrams (occupied energy levels in zero field is in orange color.

And the boundaries between different values of q_{max} are

$$B_{\nu\pm} = \frac{mE'_F}{\hbar e}\frac{1}{\nu \pm 1/2}. \tag{6B.6}$$

The energy $U_{\nu 0}$ of electrons in the k-slab corresponding to this B_ν is expressed as

$$U_{\nu 0} = \xi B_\nu \hbar\omega_c \sum_{q=0}^{\nu-1}\left(q+\frac{1}{2}\right) + n_e\frac{\hbar^2 k_z^2}{2m} = \frac{\xi B_\nu \hbar\omega_{c\nu}}{2}\nu^2 + n_e\frac{\hbar^2 k_z^2}{2m}$$
$$= \frac{\hbar\omega_{c\nu}}{2\xi B_\nu}n_{e0}^2 + \frac{\hbar^2 k_z^2}{2m}n_{e0} = \frac{h^2}{2m\delta k_z}n_{e0}^2 + \frac{\hbar^2 k_z^2}{2m}n_{e0}. \tag{6B.7}$$

This does not depend on the magnetic field and is the same as the sum of energies in k-slabs below E_F. In the region in the magnetic field $[B_{\nu+}, B_{\nu-}]$, this expression holds with replacing n_{e0} with n_e. We thus consider the quantity

$$U = \frac{h^2}{2m\delta k_z}n_e^2 + n_e\frac{\hbar^2 k_z^2}{2m} + (n_{e0}-n_e)E'_F. \tag{6B.8}$$

In the rhs, the first two terms are the extension of (6B.7) and the energy of electrons in k-slab. In the third term, the energies coming in/out the k-slab at E'_F. This term keeps U continuous even at the magnetic field of eq. (6B.6), where n_e gets a gap. Now we write E'_F as

$$E'_F = \hbar\omega_{c\nu}\nu = \hbar\frac{eB_\nu}{m}\frac{2\pi}{\delta k_z}\frac{h}{e}\frac{n_{e0}}{B_\nu} = \frac{h^2}{m}\frac{n_{e0}}{\delta k_z}. \tag{6B.9}$$

Then the variation in U is

$$\delta U = U - U_{\nu 0} = \frac{h^2}{2m\delta k_z}(n_e^2 - n_{e0}^2) + E'_F(n_{e0}-n_e) = \frac{h^2}{2m\delta k_z}(n_e - n_{e0})^2, \tag{6B.10}$$

which is more than or equal to zero.

The contribution of electrons in this k-slab to the magnetization is

$$\delta M = -\frac{\partial U}{\partial B} = -\frac{h^2}{m\delta k_z}(n_e - n_{e0})\frac{dn_e}{dB}. \tag{6B.11}$$

dn_e/dB is from eq. (6B.3)

$$\frac{dn_e}{dB} = \nu\xi \simeq \frac{E'_F}{\hbar\omega_c}\xi. \tag{6B.12}$$

Then the contribution is obtained as

$$\delta M \simeq -\frac{E'_{\rm F}}{B}(n_{\rm e} - n_{\rm e0}). \tag{6B.13}$$

While B in the denominator increases linearly, $n_{\rm e} - n_{\rm e0}$ strongly oscillates resulting in the oscillation of magnetic susceptibility.

In order to see the behavior of the total magnetization, the contribution in eq. (6B.13) should be summed up over k_z. For that, first δM is expanded in a Fourier series against the axis of B^{-1} as follows.

$$\delta M = \delta k_z \sum_{p=1}^{\infty} A_p \sin px, \quad x = 2\pi \frac{E'_{\rm F}}{\hbar\omega_{\rm c}}. \tag{6B.14}$$

We apply a mathematical identity for $-\pi < x < \pi$

$$x = e \sum_{n=1}^{\infty} \frac{(-1)^{n-1}}{n} \sin nx, \tag{6B.15}$$

and rewrite

$$\delta M = -\frac{1}{2\pi}\xi E'_{\rm F} x = \frac{1}{\pi} E'_{\rm F} \sum_p (-1)^p \frac{\sin px}{p}. \tag{6B.16}$$

Therefore the expansion coefficients are obtained as

$$A_p = \frac{1}{p\pi} E'_{\rm F} (-1)^p \frac{\xi}{\delta k_z} = (-1)^p \frac{e E'_{\rm F}}{4p\pi^3}. \tag{6B.17}$$

From the above, the summation over k_z can be written in the form of integration:

$$M = \frac{e}{4\pi^3} \sum_p \frac{(-1)^p}{p} \int_{-k_{\rm F}}^{k_{\rm F}} dk_z \cdot E'_{\rm F} \sin\left[\frac{p\pi}{\hbar\omega_{\rm c}}\left(E_{\rm F} - \frac{\hbar^2 k_z^2}{2m}\right)\right]. \tag{6B.18}$$

Here, though the magnetic field is comparatively strong, we assume the condition $\hbar\omega_{\rm c} \ll E_{\rm F}$ still holds. Then in the integrand in eq. (6B.18), $E'_{\rm F}$ varies in the section $[-k_{\rm F}, k_{\rm F}]$ as a parabola with the maximum at $k_z = 0$. On the other hand, the sine function rapidly oscillates against k_z. As a result the integration cancels out other than the region around $k_z = 0$, where $dE'_{\rm F}/dk_z \sim 0$. Hence $E'_{\rm F}$ outside the sine function can be replaced with $E_{\rm F}$. Further, applying the identity

$$\int_0^{\infty} \cos\frac{\pi}{2}x^2 dx = \int_0^{\infty} \sin\frac{\pi}{2}x^2 dx = \frac{1}{2}, \tag{6B.19}$$

the integration in (6B.18) is calculated to be

$$E_{\rm F}\left(\frac{\hbar\omega_{\rm c} m}{2p}\right)^{1/2} \sin\left(\frac{2\pi p E_{\rm F}}{\hbar\omega_{\rm c}} - \frac{\pi}{4}\right). \tag{6B.20}$$

Then we can write down the magnetization as

$$M = \frac{E_{\rm F} e^{3/2} (\hbar B)^{1/2}}{4\pi^3} \sum_p \frac{(-1)^p}{p^{3/2}} \sin\left(p\frac{2\pi E_{\rm F}}{\hbar\omega_{\rm c}} - \frac{\pi}{4}\right). \tag{6B.21}$$

The above discussion is for an ideal metal with a spherical Fermi surface. But this can be extended to general Fermi surfaces. Even in the general case, the dHvA oscillation is dominated by the region where $dE'_{\rm F}/k_z \approx 0$. Hence the magnetic field angle dependence of the dHvA oscillation (amplitude, period, etc.) gives detailed information on the Fermi surface.

Appendix 6C: Band structure of graphene

One of the ways to form a two dimensional electron system is to utilize two-dimensional crystals (two-dimensional materials). Graphene is the representative two-dimensional material. Graphene provides a good expample for the application of tight-binding calculation and we would like to see how the things go in a practical (though simplest) example.

The crystal structure of single-layer graphene is show in Fig. 6C.1(a), which is a simple honeycomb structure of carbon atoms. The diamond drawn in the figure is the unit cell and the primitive lattice vectors and the primitive reciprocal lattice vectors are written as

$$\boldsymbol{a}_1 = \begin{pmatrix} \sqrt{3}a/2 \\ a/2 \end{pmatrix}, \quad \boldsymbol{a}_2 = \begin{pmatrix} 0 \\ a \end{pmatrix}, \quad \boldsymbol{b}_1 = \begin{pmatrix} 4\pi/\sqrt{3}a \\ 0 \end{pmatrix}, \quad \boldsymbol{b}_2 = \begin{pmatrix} -2\pi/\sqrt{3}a \\ 2\pi/a \end{pmatrix}. \tag{6C.1}$$

Henceforce we calculate the electronic states of graphene under simplest approximation. Because the approximation is rough, quantitative comparison with experiments is difficult. However, the results help understanding properties of graphene, *e.g.* the Dirac points appear at the Fermi level in pure graphene. Carbon belongs to group-IV and the outmost electrons exist in the orbitals $2s$, $2p_x$, $2p_y$, $2p_z$. It is easy to see that these orbitals form sp^2-hybrids and the electronic states separate to σ-electrons (sp^2) and π-electrons (p_z). σ-electrons form the honeycome through covalent bonding and the energy bands lie at low energy region. Then the electronic states placed around the Fermi level are π-electrons. Hence we consider Schrödinger equation on π-electrons on the honeycomb lattice.

We write the equation as

$$\psi = \mathscr{H}\psi, \tag{6C.2}$$

and as Fig. 6C.1(a), we separate the lattice sites to A-sites and B-sites on different sub-lattices. We consider a kind of

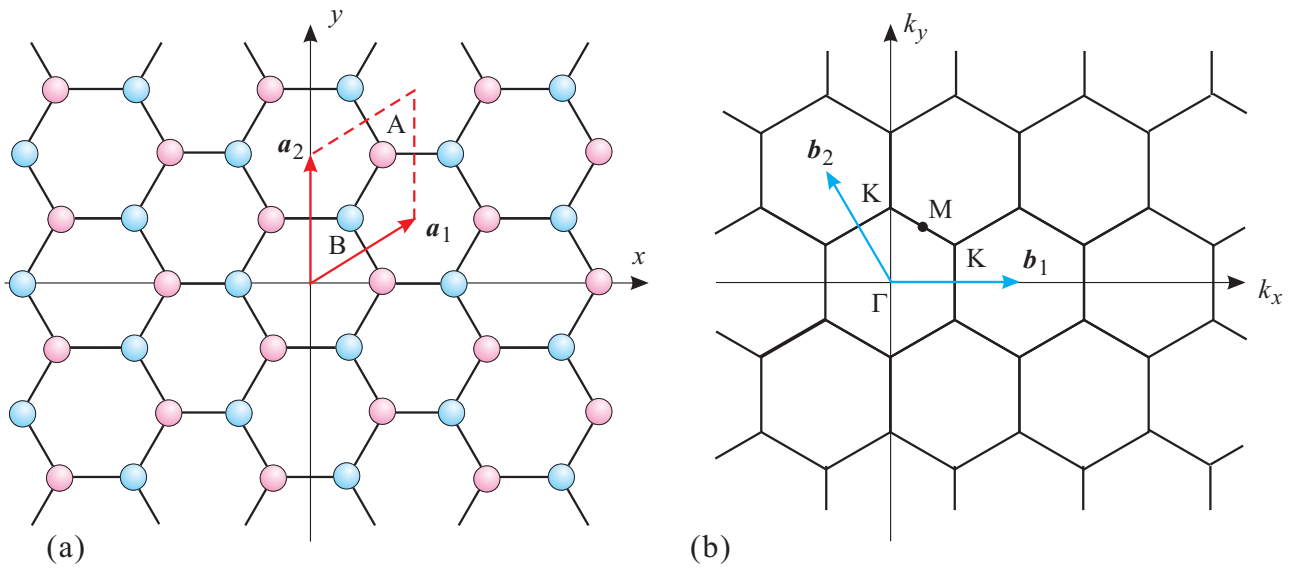

Fig. 6C.1 (a) Two dimensional cryatal structure of graphene. Carbon atoms form a honeycomb lattice. It can be also viewed as an overlap of two face-centered square lattices placed at A and B positions. (b) Reciprocal lattice of (a). $\boldsymbol{b}_1$, $\boldsymbol{b}_2$ are the primitive reciprocal lattice vector corresponding to $\boldsymbol{a}_1$, $\boldsymbol{a}_2$. The centtral point of the first Brillouin zone is Γ-point and as other points with high symmetries, K-point and M-point are indicated in the figure.

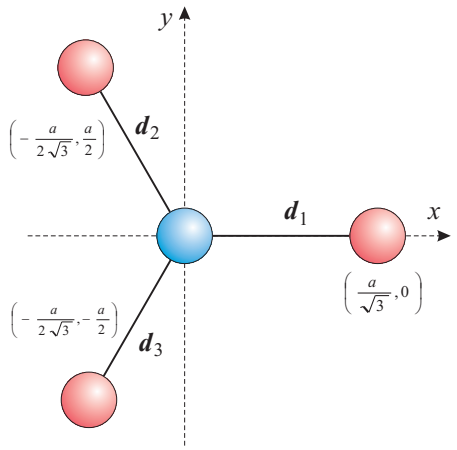

Fig. 6C.2 Vectors indicating three directional couplings between nearest neighbor carbon atoms.

tight-binding approximation between the two-sites. That is

$$\psi = \zeta_{\mathrm{A}}\psi_{\mathrm{A}} + \zeta_{\mathrm{B}}\psi_{\mathrm{B}}, \tag{6C.3}$$

$$\psi_{\mathrm{A}} = \sum_{j\in A} \exp(i\boldsymbol{k}\boldsymbol{r}_j)\phi(\boldsymbol{r}-\boldsymbol{r}_j), \tag{6C.4a}$$

$$\psi_{\mathrm{B}} = \sum_{j\in B} \exp(i\boldsymbol{k}\boldsymbol{r}_j)\phi(\boldsymbol{r}-\boldsymbol{r}_j), \tag{6C.4b}$$

where $\phi(\boldsymbol{r})$ is atomic wavefunction of π-electrons, $\boldsymbol{r}_j$ are the lattice points. Here we write the matrix elements of the Hamiltonian between the each sub-lattice wavefunctions as

$$H_{\mathrm{AA}} = \langle\psi_{\mathrm{A}}|\mathscr{H}|\psi_{\mathrm{A}}\rangle, \quad H_{\mathrm{BB}} = \langle\psi_{\mathrm{B}}|\mathscr{H}|\psi_{\mathrm{B}}\rangle, \quad H_{\mathrm{AB}} = H^*_{\mathrm{BA}} = \langle\psi_{\mathrm{A}}|\mathscr{H}|\psi_{\mathrm{B}}\rangle. \tag{6C.5}$$

And the number of atoms in the system is $2N$, that is

$$\langle\psi_{\mathrm{A}}|\psi_{\mathrm{A}}\rangle = \langle\psi_{\mathrm{B}}|\psi_{\mathrm{B}}\rangle = N. \tag{6C.6}$$

Let $\langle\psi_{\mathrm{A}}|\psi_{\mathrm{B}}\rangle$ be zero. We substitute (6C.3) to (6C.2). The condition of have non-trivial $(\zeta_{\mathrm{A}}, \zeta_{\mathrm{B}})$ givies the cecular equation

$$\begin{vmatrix} H_{\mathrm{AA}} - NE & H_{\mathrm{AB}} \\ H_{\mathrm{BA}} & H_{\mathrm{BB}} - NE \end{vmatrix} = 0. \tag{6C.7}$$

Lastly

$$E = (2N)^{-1}\left(H_{\mathrm{AA}} + H_{\mathrm{BB}} \pm \sqrt{(H_{\mathrm{AA}} - H_{\mathrm{BB}})^2 + 4|H_{\mathrm{AB}}|^2}\right) \equiv h_{\mathrm{AA}} \pm |h_{\mathrm{AB}}|, \tag{6C.8}$$

where we have used $H_{\mathrm{AA}} = H_{\mathrm{BB}}$, which comes from the symmetry, and we use lower cases for the quantities per atom with being devided by $(2N)^{-1}$.

$$H_{\mathrm{AB}} = \sum_{l\in\mathrm{A}, j\in\mathrm{B}} \exp\left[i\boldsymbol{k}(\boldsymbol{r}_j - \boldsymbol{r}_l)\right] \langle\phi(\boldsymbol{r}-\boldsymbol{r}_l)|\mathscr{H}|\phi(\boldsymbol{r}-\boldsymbol{r}_j)\rangle_{\boldsymbol{r}}. \tag{6C.9}$$

We further approximate that the off-diagonal matrix elements of $\mathscr{H}$ just exist between the nearest neighbor sites. For the calculation we take the atom indicated as A in Fig. 6C.1(a) as the center atom. The vectors from A to the nearest neighbor atoms 1, 2, 3 are $\boldsymbol{d}_i (i = 1, 2, 3)$ respectively. As is apparent from the figure,

$$\boldsymbol{k}\cdot\boldsymbol{d}_1 = \frac{k_x a}{\sqrt{3}}, \quad \boldsymbol{k}\cdot\boldsymbol{d}_2 = \left(-\frac{k_x}{2\sqrt{3}} + \frac{k_y}{2}\right)a, \quad \boldsymbol{k}\cdot\boldsymbol{d}_3 = \left(-\frac{k_x}{2\sqrt{3}} - \frac{k_y}{2}\right)a, \tag{6C.10}$$

where $a = |\boldsymbol{a}_1| = |\boldsymbol{a}_2|$. The terms $\langle\phi(\boldsymbol{r}-\boldsymbol{r}_l)|\mathscr{H}|\phi(\boldsymbol{r}-\boldsymbol{r}_j)\rangle_{\boldsymbol{r}}$ should be equal due to the symmetry and we write it as ξ. Consequently the residual resonant integral from the crystal structure is the repetition of the above and

$$h_{\mathrm{AB}} = \left(\sum_{j=1}^{3} \exp(i\boldsymbol{k}\cdot\boldsymbol{d}_j)\right)\xi. \tag{6C.11}$$

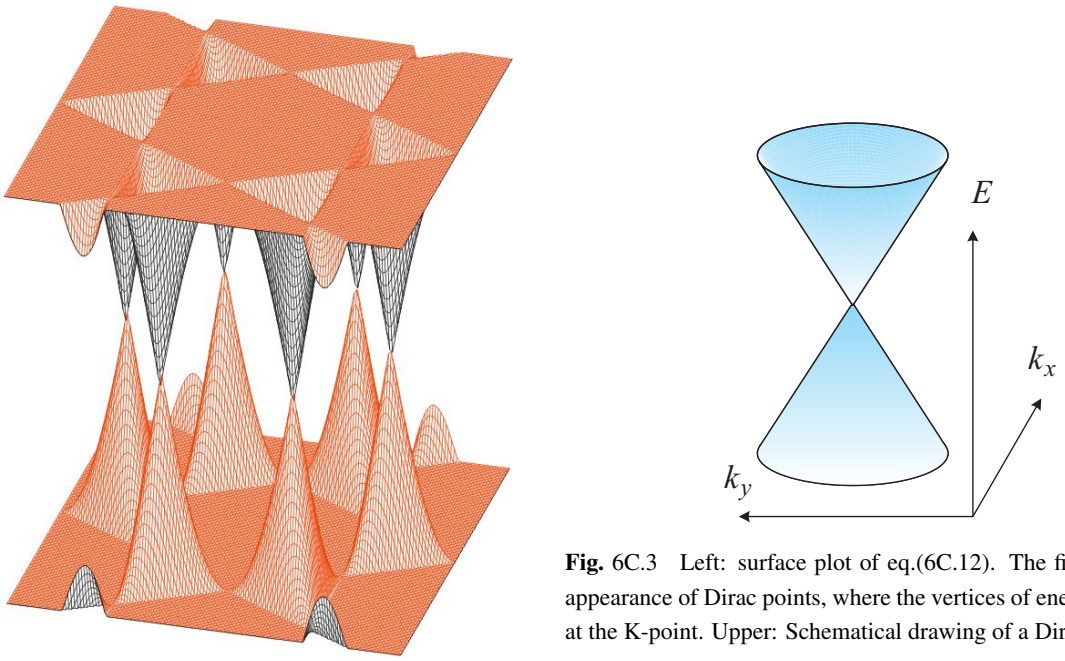

Fig. 6C.3 Left: surface plot of eq.(6C.12). The figure shows the appearance of Dirac points, where the vertices of energy corns crash at the K-point. Upper: Schematical drawing of a Dirac point.

Substituting eqs.(6C.10), (6C.11) into eq.(6C.8), we get the following expressio for the energy.

$$E = h_{\mathrm{AA}} \pm \xi \sqrt{1 + 4\cos\frac{\sqrt{3}k_x a}{2}\cos\frac{k_y a}{2} + 4\cos^2\frac{k_y a}{2}}. \tag{6C.12}$$

The second term is the perturbation from the nearest neighbor resonant integral, which vanishes at K-point in the reciprocal space

$$(k_x, k_y) = \left(0, \pm\frac{4\pi}{3a}\right), \quad \left(\frac{2\pi}{\sqrt{3}a}, \pm\frac{2\pi}{3a}\right), \quad \left(-\frac{2\pi}{\sqrt{3}a}, \pm\frac{2\pi}{3a}\right). \tag{6C.13}$$

We write $k_y = 4\pi/3a$ and around $k_x = 0$(one of the K-points), eq. (6C.12) can be approximated as

$$E\left(k_x, \frac{4\pi}{3a}\right) \approx h_{\mathrm{AA}} + \frac{\sqrt{3}\xi a}{2}|k_x|. \tag{6C.14}$$

Namely, at the K-point the upper band has a lower pointed shape. Because the same for the lower band and as a result, at the K-point, as shown in Fig. 6C.3, the band structure called **Dirac point**, which has no energy gap, no effective mass, appears.

Equation (6C.12) is for a very simplified model. Just like a cosine band appeared in the tight-binding model in one-dimension, the model itself does not have realistic meaning. However the model tells that the reason why we have the Dirac points at K-points is that the exsittence of three equivalent resonant integrals in eq. (6C.11). The inference holds for the band calculation with any level precision since it is based on the symmetry. That meas the K-points in real graphene are really Dirac points.

References

[1] P M C Rourke, A F Bangura, T M Benseman, M Matusiak, J R Cooper, A Carrington, and N E Hussey. A detailed de haas-van alphen effect study of the overdoped cuprate $\mathrm{tl_2ba_2cuo_{6+\delta}}$. *New Journal of Physics*, Vol. 12, No. 10, p. 105009, October 2010.

[2] Hidetoshi Fukuyama. Theory of orbital magnetism of bloch electrons: Coulomb interactions. *Progress of Theoretical Physics*, Vol. 45, No. 3, pp. 704–729, March 1971.

[3] Masao Ogata and Hidetoshi Fukuyama. Orbital magnetism of bloch electrons i. general formula. *Journal of the Physical Society of Japan*, Vol. 84, No. 12, p. 124708, December 2015.

[4] Masao Ogata. Orbital magnetism of bloch electrons: II. application to single-band models and corrections to landau–peierls susceptibility. *Journal of the Physical Society of Japan*, Vol. 85, No. 6, p. 064709, June 2016.

[5] Masao Ogata. Orbital magnetism of bloch electrons: III. application to graphene. *Journal of the Physical Society of Japan*, Vol. 85, No. 10, p. 104708, October 2016.

[6] J. W. McClure. Diamagnetism of graphite. *Phys. Rev.*, Vol. 104, pp. 666–671, Nov 1956.

[7] Bogdan Semenenko and Pablo Esquinazi. Diamagnetism of bulk graphite revised. *Magnetochemistry*, Vol. 4, No. 4, p. 52, November 2018.

[8] 越野幹人. グラフェンにおける巨大な軌道反磁性 (最近の研究から). 日本物理学会誌, Vol. 65, No. 1, pp. 21–25, 2010.

[9] Mikito Koshino, Yasunori Arimura, and Tsuneya Ando. Magnetic field screening and mirroring in graphene. *Phys. Rev. Lett.*, Vol. 102, p. 177203, Apr 2009.

[10] Mikito Koshino and Tsuneya Ando. Orbital diamagnetism in multilayer graphenes: Systematic study with the effective mass approximation. *Phys. Rev. B*, Vol. 76, p. 085425, Aug 2007.

[11] W. Heisenberg. Mehrkörperproblem und resonanz in der quantenmechanik. *Zeitschrift für Physik*, Vol. 38, No. 6-7, pp. 411–426, June 1926.

[12] L D Landau and E. M. Lifshitz. *Quantum Mechanics: Non-Relativistic Theory (English Edition)*. Butterworth-Heinemann, 12 1981.

[13] Charles Kittel. *Quantum Theory of Solids 2E Rev P*. WILEY, 3 1987.